Chinese Chemical Letters 35 (2024) 109133

Contents lists available at ScienceDirect

Chinese Chemical Letters

journal homepage: www.elsevier.com/locate/cclet

FRET-based two-photon benzo[*a*] phenothiazinium photosensitizer for fluorescence imaging-guided photodynamic therapy

Yiling Li[a,1], Zekun Gao[b,1], Xiuxiu Yue[a], Minhuan Lan[a,*], Xiuli Zheng[b,*], Benhua Wang[a], Shuang Zhao[c], Xiangzhi Song[a,*]

[a] College of Chemistry & Chemical Engineering, Central South University, Changsha 410083, China
[b] Key Laboratory of Photochemical Conversion and Optoelectronic Materials and City U-CAS Joint Laboratory of Functional Materials and Devices, Technical Institute of Physics and Chemistry, Chinese Academy of Sciences, Beijing 100190, China
[c] Department of Dermatology, Xiangya Hospital, Central South University, Changsha 410083, China

ARTICLE INFO

Article history:
Received 23 June 2023
Revised 12 September 2023
Accepted 20 September 2023
Available online 9 October 2023

Keywords:
Photodynamic therapy
Two-photon excitation
FRET-based photosensitizer
Singlet oxygen
Near-infrared fluorescence

ABSTRACT

To overcome the conflict between the long-wavelength excitation and high singlet oxygen quantum yield of photosensitizers, we conjugated a two-photon fluorophore, tetrahydroquinoxaline coumarin (TQ), and an efficient photodynamic therapeutic agent, benzo[*a*]phenothiazinium (NBS-NH_2), through a hexamethylene linker to build a two-photon photosensitizer, TQ-NBS. In TQ-NBS, TQ served as an energy donor and NBS-NH_2 acted as an energy acceptor; and TQ-NBS was a Förster resonance energy transfer (FRET) cassette with a 92.8% efficiency. The large two-photon absorption cross-section of TQ allowed photosensitizer TQ-NBS to work in a 900 nm two-photon excitation (TPE) mode, which greatly benefited the deep tissue penetration in PDT treatment. Meanwhile, the excellent phototoxicity and near-infrared fluorescence of NBS-NH_2 was kept in TQ-NBS under a TPE mode *via* a FRET process. Photosensitizer TQ-NBS exhibited a high phototoxic efficacy in living cells and tumor-bearing mice.

Compared with traditional clinical treatments (*e.g.*, chemotherapy [1], radiotherapy [2], and surgery [3]), photodynamic therapy (PDT) has emerged as a promising cancer treatment with the advantages of high selectivity, no drug resistance, and negligible invasiveness [4–7]. In PDT treatment, photosensitizers absorb light to be excited to triplet state; and a triplet-triplet energy transfer between the excited molecules of the photosensitizers and the O_2 molecules generates singlet oxygen ($^1O_2$), which are highly destructive to cancer cells [8–10]. Therefore, under light irradiation and in the presence of O_2, photosensitizers display efficient phototoxicity to cancer cells and tumors with high selectivity [11,12]. Since light is necessary for PDT treatment, long-wavelength photons are desirable because of their deep tissue penetration [13,14]. Consequently, researchers have made a lot of efforts to develop photosensitizers having long-wavelength absorptions in optical window (600–900 nm). According to Fermi's golden rule, however, there is a limit for $^1O_2$ quantum yield of photosensitizers with an absorption mainly in near-infrared (NIR) region [15]. The longer the absorption wavelength is, the lower the $^1O_2$ quantum yield of photosensitizers is [9,16]. Moreover, NIR photosensitizers usually have complicated chemical structures and poor photostability [17,18].

Compared with one-photon excitation (OPE), two-photon excitation (TPE) technology employs with two simultaneous photons with longer wavelength to excite the fluorophore, and thereby having deeper tissue penetration and higher imaging resolution [19–21]. Recently, TPE technology has been becoming attractive in PDT because deep red or NIR pulsed laser can be used to illuminate photosensitizers to produce $^1O_2$ to induce cell death [22]. Besides, TPE has a high spatial resolution of fluorescence imaging and minimal photodamage to the surrounding healthy tissue [23–26]. However, intrinsic TPE photosensitizers usually have small two-photon absorption cross-sections, which results in the low $^1O_2$ generation efficiency [27,28]. In order to solve the above issues, Förster resonance energy transfer (FRET) mechanism has been used to design TPE-PDT by conjugating a photosensitizer with an energy donor having large two-photon absorption cross-sections such as semiconductor quantum dots [29], carbon dots [30,31], and polymers [32]. However, these complex TPE-PDT agents are subjected to uncontrollable surface modification, biosafety concern, or poor water solubility [33–36]. Therefore, developing small organic

* Corresponding authors.
E-mail addresses: minhuanlan@csu.edu.cn (M. Lan), zhengxiuli@mail.ipc.ac.cn (X. Zheng), xzsong@csu.edu.cn (X. Song).
[1] These authors contributed equally to this work.

https://doi.org/10.1016/j.cclet.2023.109133
1001-8417/

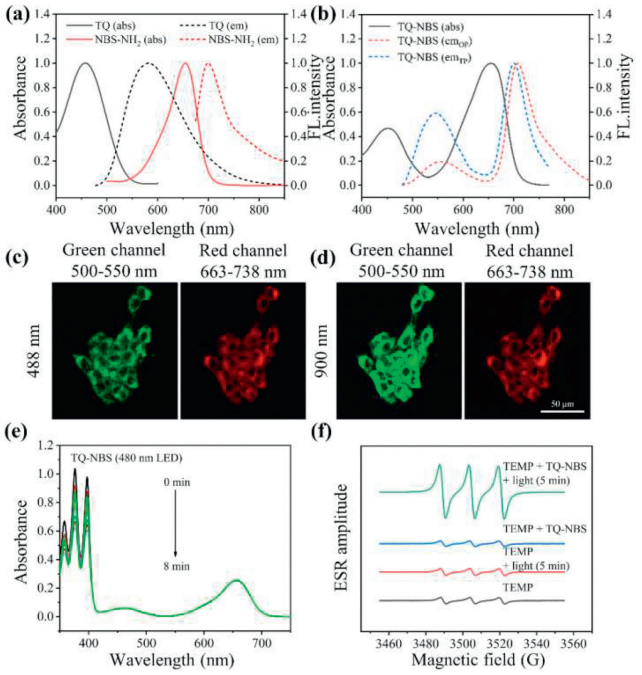

Fig. 1. (a) Normalized absorption and emission spectra of NBS-NH_2 and TQ in MeOH. (b) Normalized absorption and emission spectra of TQ-NBS in MeOH, Ex (OPE) = 450 nm, Ex (TPE) = 900 nm. (c) OPE and (d) TPE fluorescence images of 4T1 cells incubated with TQ-NBS (5 μmol/L), Ex (OPE) = 488 nm, Ex (TPE) = 900 nm. Scale bar: 50 μm. (e) Time-dependent ultraviolet–visible absorption spectra of the mixture of ABDA and TQ-NBS in MeOH upon LED (480 nm, 20 mW/cm^2) irradiation. (f) ESR signals of DMPO for $^1O_2$ characterization under 900 nm light irradiation (100 mW/cm^2).

molecular TPE photosensitizers with good biocompatibility through FRET mechanism is very necessary.

Benzo[*a*]phenothiazinium dyes (NBS) are effective photosensitizers for PDT treatment because they have an intense red absorption and a NIR fluorescence, efficient $^1O_2$ generation ability, and good biocompatibility [37–39]. Though the absorption of NBS-NH_2 (λ_{max} = 655 nm) is in the optical window, the penetration ability of the excitation light limits its effectiveness in the treatment of tumors with large size or in deep position to some extent. Recently, we reported a tetrahydroquinoxaline coumarin dye (TQ) [40], which has a large two-photon absorption cross-section over 100 GM and an emission with λ_{max} = 585 nm (Fig. 1a). Considering the large spectral overlapping between the absorption of NBS-NH_2 and the emission of TQ, we expected to build an efficient FRET cassette with NBS-NH_2 and TQ in which TQ acts as the energy donor and NBS-NH_2 servers as the energy acceptor. Therefore, we might take the respective advantage of NBS-NH_2 and TQ to construct a novel FRET-based TPE photosensitizer (TQ-NBS). As demonstrated in Scheme 1, TQ and NBS-NH_2 were conjugated through a hexamethylene linker to give TQ-NBS. Under a two-photon excitation, TQ-NBS can simultaneously generate $^1O_2$ and NIR fluorescence, achieving two-photon imaging-guided PDT for cancer cells.

The preparation of TQ-NBS was depicted in Scheme S1 (Supporting information). The chemical structure of TQ-NBS was characterized by nuclear magnetic resonance (NMR) and high-resolution mass spectral analysis. Next, we investigated the optical properties of TQ-NBS. As shown in Fig. 1b, TQ-NBS showed two intensive absorption bands centered at 455 and 655 nm, assigned to TQ and NBS, respectively. Meanwhile, TQ-NBS exhibited two fluorescence peaks at 555 and 705 nm under OPE, indicating the occurrence of the FRET process. The FRET efficiency in TQ-NBS was determined to be 92.8%, which was much higher than that of most

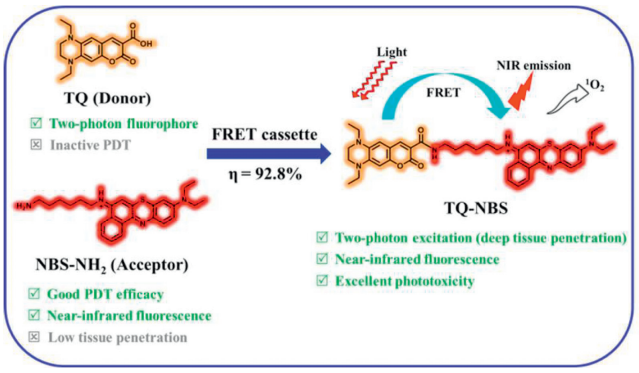

Scheme 1. Schematic diagram of the design strategy of TQ-NBS *via* FRET process.

of the previously reported FRET-based photosensitizers [12,41-43]. Moreover, we used TPE to study the optical properties of TQ-NBS. As shown in Fig. 1b, two fluorescence peaks at 545 and 700 nm were observed under 900 nm pulsed laser excitation, clearly proving the existence of the FRET process in TQ-NBS.

The chemical stability of TQ-NBS was investigated in the presence of different biologically relevant analytes. As shown in Fig. S1 (Supporting information), the fluorescence intensity at 705 nm of TQ-NBS hardly changed with the addition of these analytes, revealing that TQ-NBS was chemically stable. Next, we used TQ-NBS to incubate living 4T1 cells and investigate its fluorescence imaging performance *in vitro*. As indicated in Fig. 1c, strong fluorescence signals in both green and red channels were seen from inside cells when illuminated under a 488 nm laser (OPE). As expected, cells under a 900 nm laser irradiation (TPE) also gave strong green and red fluorescence signals (Fig. 1d). It was seen that the TPE imaging resolution was much higher than the OPE one because TPE can minimize the light scattering and reduce endogenous absorption of biological tissues [26,44].

To evaluate the $^1O_2$ generation ability of TQ-NBS, 9,10-anthracenediyl-bis(methylene)dimalonic acid (ABDA) was used as the $^1O_2$ indicator. First, a 480 nm light-emitting diode (LED) was used as a light source to illuminate the mixture of TQ-NBS and ABDA. Under the light irradiation, the absorbance of ABDA sharply decreased after 8 min irradiation, suggesting TQ-NBS could produce $^1O_2$ *via* the FRET process (Fig. 1e and Fig. S2 in Supporting information). The $^1O_2$ quantum yield of TQ-NBS was determined to be 7.5%. To verify the $^1O_2$ generation capability of TQ-NBS under TPE, electron spin resonance (ESR) spectroscopy was performed using 2,2,6,6-tetramethylpiperidine (TEMP) as the spin trapping agent for $^1O_2$. As shown in Fig. 1f, the ESR signals barely changed in the presence or absence of TQ-NBS without light illumination. Under TPE illumination (900 nm pulsed laser), in contrast, the signals of characteristic paramagnetic adducts were clearly observed, indicating the generation of $^1O_2$.

Furthermore, the $^1O_2$ generation capability of TQ-NBS in living cells was evaluated using 2,7-dichlorofluorescein diacetate (DCFH-DA) as an indicator. A 480 nm LED was used as the light sources. 4T1 cells were incubated with TQ-NBS and DCFH-DA for 30 min. Meanwhile, cells were incubated with phosphate buffered saline (PBS) and DCFH-DA as the control. As shown in Fig. S3 (Supporting information), bright green fluorescence was observed from TQ-NBS-pretreated cells after 20 min light illumination. Without light illumination, however, no obvious fluorescence was detected from TQ-NBS-pretreated cells. For the PBS-treated control group, cells gave off no fluorescence no matter there was a light illumination or not.

Next, calcein AM/propidium iodide (AM/PI) co-staining assay was carried out to evaluate the photocytotoxicity of TQ-NBS. As

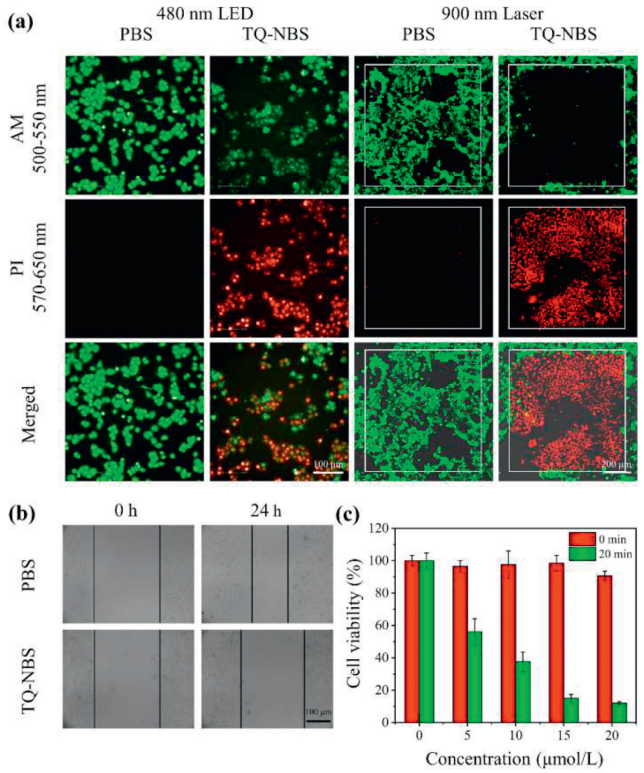

Fig. 2. (a) Fluorescence images of 4T1 cells stained with calcein AM/PI under 480 nm LED (20 mW/cm^2) and 900 nm laser (1.5 W/cm^2) illumination for 20 min, respectively, Ex = 460–490 nm. Scale bar: 100 μm for left two columns and 200 μm for right two columns. (b) The scratch assay of 4T1 cells after 480 nm LED (20 mW/cm^2) illumination for 20 min. (c) The cell viability of 4T1 cells in the presence of TQ-NBS (0–20 μmol/L) with or without 480 nm LED (20 mW/cm^2) illumination for 20 min. Error bars: mean ± standard deviation (SD) (n = 6).

shown in Fig. 2a, the irradiation under a 480 nm LED on TQ-NBS-treated cells resulted in strong fluorescence in the red channel and reduced fluorescence in the green channel. In the absence of TQ-NBS, the cells only exhibited strong fluorescence in the green channel. We were pleased that the irradiation under a 900 nm pulsed laser also gave the same results. These results proved that TQ-NBS could exhibit high phototoxicity under both OPE and TPE modes. Additionally, the scratch assay was performed on 4T1 cells to further visualize the PDT effect of TQ-NBS. As shown in Fig. 2b, the wound gap became wider after 24 h when TQ-NBS-treated cells were irradiated under a LED light. Regarding the PBS-treated control group, the wound gap was narrowed after 24 h. The wound healing experiments indicated that TQ-NBS had excellent PDT effect on inhibiting cell migration. The cytotoxicity of TQ-NBS was further determined using the MTT assay. As shown in Fig. 2c, the cytotoxicity of TQ-NBS was negligible in the dark. Under a light irradiation for 20 min, TQ-NBS showed strong dose-dependent phototoxicity and the cell viability was less than 20% when cells were treated with 15 μmol/L TQ-NBS.

To confirm whether the PDT effect of TQ-NBS arises from the generated $^1O_2$, we used annexin V-fluorescein isothiocyanate (FITC) and PI as indicators to determine the cell death pathways [45]. As shown in Fig. 3, TQ-NBS-incubated cells exhibited strong fluorescence in both green and red channels after the light irradiation, indicating the cell apoptosis and necrosis [46]. It is known that vitamin C can effectively consume $^1O_2$ [47]. Then, we used vitamin C to incubate TQ-NBS-treated cells and later illuminated cells with the LED light. It was found that the fluorescence in both green and red channels was dramatically weakened. These results

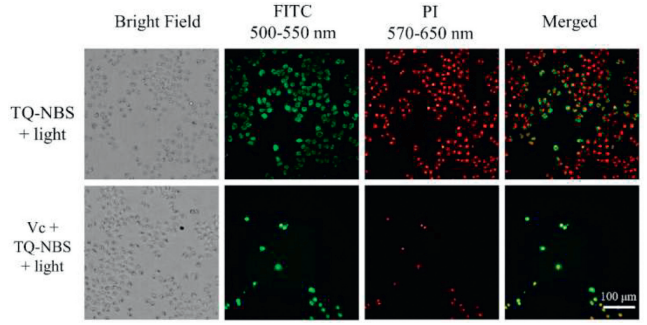

Fig. 3. Bright field and fluorescence images of TQ-NBS-treated cells co-stained with annexin V-FITC and PI, respectively, after 20 min light irradiation (480 nm LED, 20 mW/cm^2) in the absence or presence of vitamin C. Scale bar: 100 μm.

strongly supported the fact that the apoptosis of TQ-NBS-treated cells was caused by $^1O_2$.

The *in vivo* PDT efficiency of TQ-NBS was investigated in 4T1 tumor-bearing mice. All related animal experiments were performed according to guidelines approved by the Ethics Committee of Hunan Normal University. As shown in Fig. 4a, PBS-treated tumors grew very fast after 14 days and the light irradiation had negligible effect on the tumor size. Without light irradiation, TQ-NBS-treated tumors still displayed a fast growth. In a sharp contrast, the growth of TQ-NBS-treated tumors was significantly inhibited under a light irradiation. Furthermore, the body weight of tumor-bearing mice did show negligible changes, and no distinct damage and inflammatory lesions were observed in the central organs after 14 days of treatment (Figs. 4b and c; Fig. S4 in Supporting information). These *in vivo* experiments suggested that TQ-NBS exhibited good biocompatibility and effective therapeutic effects in the tumor-bearing mice.

In conclusion, a small organic molecular two-photon photosensitizer, TQ-NBS, was developed based on FRET mechanism. Under TPE light irradiation, TQ-NBS displayed NIR fluorescence and good PDT efficacy in living cells. The high penetration ability of TPE and the high FRET efficiency make photosensitizer TQ-NBS a good photosensitizer for the potential deep cancer treatment. This work also

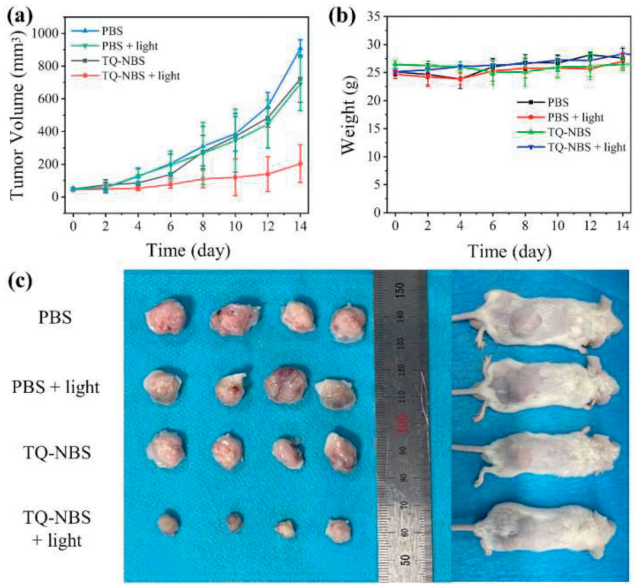

Fig. 4. (a) Plots of tumor volume of mice *versus* time. (b) Plots of body weight of mice *versus* time. (c) Images of tumors and mice after 14 days. Mice were treated with PBS, TQ-NBS (5 μmol/L), respectively, with and without light irradiation.

provides an inspiration for the development of new TPE photosensitizers in the future.

Declaration of competing interest

The authors declare that they have no known competing financial interests or personal relationships that could have appeared to influence the work reported in this paper.

Acknowledgments

This work was supported by National Key Research and Development Program of China (No. 2022YFA1207600) and National Natural Science Foundation of China (Nos. 22178395, 62175262 and 62005294).

Supplementary materials

Supplementary material associated with this article can be found, in the online version, at doi:10.1016/j.cclet.2023.109133.

References

[1] S. Qin, Y. Cheng, Q. Lei, et al., Biomaterials 171 (2018) 178–197.
[2] Z. Liu, Z. Xie, W. Li, et al., J. Nanobiotechnol. 19 (2021) 160.
[3] A. Kudo, M. Shinoda, S. Ariizumi, et al., J. Cancer Res. Clin. Oncol. 146 (2020) 2949–2956.
[4] S. Houthoofd, M. Vuylsteke, S. Mordon, I. Fourneau, Photodiagn. Photodyn. Ther. 29 (2020) 101568.
[5] J. Karges, Angew. Chem. Int. Ed. 61 (2022) e202112236.
[6] S. Liao, M. Cai, R. Zhu, et al., Mol. Pharm. 20 (2023) 875–885.
[7] F. Xu, H. Li, Q. Yao, et al., Chem. Sci. 10 (2019) 10586–10594.
[8] F. Bolze, S. Jenni, A. Sour, V. Heitz, Chem. Commun. 53 (2017) 12857–12877.
[9] G. Feng, G. Zhang, D. Ding, Chem. Soc. Rev. 49 (2020) 8179–8234.
[10] E. Pang, S. Zhao, B. Wang, et al., Coord. Chem. Rev. 472 (2022) 214780.
[11] D. Chen, Q. Xu, W. Wang, et al., Small 17 (2021) 2006742.
[12] L. Shi, P. Zhang, X. Liu, et al., Adv. Mater. 34 (2022) 2206659.
[13] X. Zhao, Y. Yang, Y. Yu, et al., Chem. Commun. 55 (2019) 13542–13545.
[14] B. Zheng, D. Zhong, T. Xie, et al., Chem 7 (2021) 1615–1625.
[15] M.A. Manae, A. Hazra, Phys. Chem. Chem. Phys. 24 (2022) 13266–13274.
[16] K. Hayashi, M. Nakamura, H. Miki, et al., Adv. Funct. Mater. 24 (2014) 503–513.
[17] I.W. Badon, C. Kim, J.M. Lim, et al., J. Mater. Chem. B 10 (2022) 1196–1209.
[18] B. Yin, Q. Qin, Z. Li, et al., Nano Today 45 (2022) 101550.
[19] X. Zhang, F. Yang, T. Ren, et al., Chin. Chem. Lett. 34 (2023) 107835.
[20] X. He, B. Situ, M. Gao, et al., Small 15 (2019) 1905080.
[21] D. Chen, W. Qin, H. Fang, et al., Chin. Chem. Lett. 30 (2019) 1738–1744.
[22] S. Wang, H. Chen, J. Liu, et al., Adv. Funct. Mater. 30 (2020) 2002546.
[23] B. Gu, W. Wu, G. Xu, et al., Adv. Mater. 29 (2017) 1701076.
[24] Y. Yang, H. Zhong, B. Wang, et al., Chin. Chem. Lett. 34 (2023) 107674.
[25] T. Wu, X. Lu, Z. Yu, et al., J. Mater. Chem. B 11 (2023) 1213–1221.
[26] Y. Zhou, D. Zhang, G. He, et al., J. Mater. Chem. B 9 (2021) 1009–1017.
[27] M. Galland, T. Le Bahers, A. Banyasz, et al., Chem. Eur. J. 25 (2019) 9026–9034.
[28] W.R. Dichtel, J.M. Serin, C. Edder, et al., J. Am. Chem. Soc. 126 (2004) 5380–5381.
[29] J. Sun, Q. Xin, Y. Yang, et al., Chem. Commun. 54 (2018) 715–718.
[30] N. Naskar, W. Liu, H. Qi, et al., ACS Appl. Mater. Interfaces 14 (2022) 48327–48340.
[31] K. Yang, C. Wang, C. Liu, et al., J. Mater. Sci. 54 (2019) 3383–3391.
[32] C. Wu, Q. Xu, Macromol. Rapid Commun. 30 (2009) 504–508.
[33] R.L. Pinals, L. Chio, F. Ledesma, M.P. Landry, Analyst 145 (2020) 5090–5112.
[34] W. Qiu, M. Liang, Y. Gao, et al., Theranostics 11 (2021) 9652–9666.
[35] R. Timor, H. Weitman, N. Waiskopf, et al., ACS Appl. Mater. Interfaces 7 (2015) 21107–21114.
[36] Z. Xu, L. Mei, Y. Shi, et al., Biomacromolecules 23 (2022) 2778–2784.
[37] J.W. Foley, X. Song, T.N. Demidova, et al., J. Med. Chem. 49 (2006) 5291–5299.
[38] M. Li, J. Xia, R. Tian, et al., J. Am. Chem. Soc. 140 (2018) 14851–14859.
[39] M. Li, T. Xiong, J. Du, et al., J. Am. Chem. Soc. 141 (2019) 2695–2702.
[40] L. He, H. Xiong, B. Wang, et al., Anal. Chem. 92 (2020) 11029–11034.
[41] H. Cao, L. Wang, Y. Yang, et al., Angew. Chem. Int. Ed. 57 (2018) 7759–7763.
[42] J. Liu, L. Wang, R. Shen, et al., Spectrochim. Acta Part A 274 (2022) 121083.
[43] J. Wang, J. Li, Z. Yu, et al., Anal. Chem. 94 (2022) 14029–14037.
[44] V. Juvekar, H.W. Lee, D.J. Lee, H.M. Kim, Trends Anal. Chem. 157 (2022) 116787.
[45] Y. Zhao, Y. Liu, W. Wang, et al., J. Funct. Foods 49 (2018) 412–423.
[46] S. Banesh, V. Trivedi, Mol. Biotechnol. 63 (2021) 992–1003.
[47] A. Zhitkovich, Chem. Res. Toxicol. 33 (2020) 2515–2526.